ChemComm

Check for updates

Facile synthesis of epsilon iron oxides *via* spray drying for millimeter-wave absorption†

Gi Ryeon Jo,[ab] Min Byeol Yun,[ab] Yeong Hun Son,[ab] Byeongjin Park, [iD][c] Jung-Goo Lee,[a] Young-Guk Kim, [iD][a] Young-Guk Son*[b] and Youn-Kyoung Baek [iD]*[a]

A simple, scalable spray drying method was developed for high-yield epsilon iron oxide (ε-Fe$_2$O$_3$) synthesis. The ε-Fe$_2$O$_3$ particle size can be tailored by varying the annealing temperature and molar ratio of Fe/Si, producing a high-purity ε-phase. This strategy also enables ferromagnetic resonance tuning, making it potentially usable in millimeter-wave absorbers.

High-coercivity oxide magnets have been intensively developed for various applications, such as permanent magnets, information storage systems, electromagnetic interference (EMI) shielding devices, and magnetic recording media.[1–3] In particular, epsilon iron oxide (ε-Fe$_2$O$_3$) has garnered considerable attention because of its high coercive field of more than 20 kOe at room temperature, which is 3–4 times higher than those of ferrites and similar to those of rare-earth permanent magnets.[4,5] The large coercive field of the ε-phase is attributed to the orthorhombic structure with a large magnetocrystalline anisotropy (7.7×10^6 erg·cm^{-3}), which is in contrast to the other iron oxide polymorphs (α and γ-Fe$_2$O$_3$), which have isotropic crystal structures.[4,6] In addition, ε-Fe$_2$O$_3$ exhibits electromagnetic (EM) wave absorption at a high frequency ($\sim$182 GHz) because the zero-field ferromagnetic resonance is proportional to its strong magnetic anisotropy field.[7,8] The substitution of nonmagnetic elements with Fe sites enables tunable absorption in the millimeter-wave region (30–300 GHz).[8–10]

Thus, several studies have been conducted to produce high-purity ε-Fe$_2$O$_3$. The ε-phase can be obtained in nanoparticle (NP) form rather than bulk form because it is an intermediate between γ-Fe$_2$O$_3$ and α-Fe$_2$O$_3$.[3,4,11] Therefore, a crucial requirement for obtaining single-phase ε-Fe$_2$O$_3$ is to control the

particle size in a specific range (8–40 nm) that makes the ε-phase stable.[5] Most commonly, pure ε-Fe$_2$O$_3$ NPs are fabricated by the reverse-micelle and sol–gel method,[12–14] rapid sol-gel method,[15] and impregnation of mesoporous templates with Fe salts.[3,4] These approaches prevent the excessive growth of crystallites by using a silica matrix, surfactant, or porous template, resulting in a high-purity ε-phase. However, such methods involve multiple time-consuming steps, produce low yields, and require expensive sacrificial templates, which limit large-scale production and practical applications. Therefore, a facile and scalable technique for producing high-purity ε-Fe$_2$O$_3$ should be developed.

Spray drying has been widely used for the industrial manufacturing of dried fine powders for pharmaceuticals, foods, and chemicals.[16] This process involves instant and continuous evaporation of aerosol droplets, enabling the production of powders in a single step without additional washing.[16] Furthermore, this approach has no limit in terms of the combination of multiple compounds in particle form;[16] this makes the synthesis of composites with dispersed elemental Fe and Si possible without the use of templates or surfactants. Therefore, this method has great potential as a high-yield technique for producing pure ε-phase. To the best of our knowledge, there have been no reports on the synthesis of ε-Fe$_2$O$_3$ *via* spray drying.

In this study, a simple and scalable method was developed for the synthesis of high-purity ε-Fe$_2$O$_3$ *via* spray drying. Single-phase ε-Fe$_2$O$_3$ NPs were fabricated by controlling the annealing temperature and precursor molar ratio. The ferromagnetic resonance characteristics of the resulting iron oxide were adjusted in the millimeter-wave region by simple substitution with nonmagnetic metal ions. The results provide a basis for the industrial production of magnetic NPs as millimeter-wave absorbers.

Fig. 1(a) shows a diagram illustrating the spray-assisted synthesis of high-purity ε-Fe$_2$O$_3$. We performed the spray drying of a solution mixture of Fe salt (Fe(NO$_3$)$_3$·9H$_2$O) and a silica precursor (tetraethoxysilane, TEOS) in a hot chamber, followed by post-heat treatment and sequential washing. As shown in

a Powder Materials Division, Korea Institute of Materials Science, Changwon, 51508, South Korea. E-mail: ykbaek@kims.re.kr

b School of Materials Science & Engineering, Pusan National University, Busan, 46241, South Korea. E-mail: ykson@pusan.ac.kr

c Composites Research Division, Korea Institute of Materials Science, Changwon, 51508, South Korea

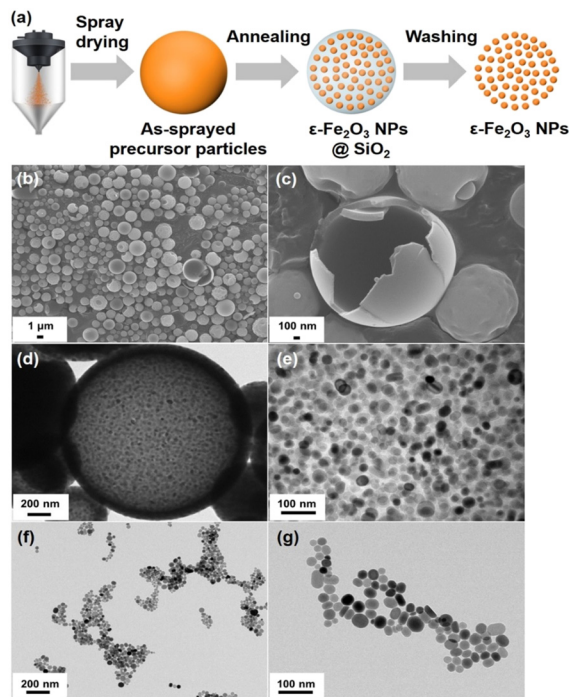† Electronic supplementary information (ESI) available. See DOI: https://doi.org/10.1039/d2cc03168j

Fig. 1 (a) Schematic illustration of the preparation of ε-Fe$_2$O$_3$ NPs *via* spray drying. (b) and (c) Scanning electron microscopy (SEM) images of as-spray-dried precursor particles with a precursor molar ratio (Fe/Si) of 0.4 : 1. (d) and (e) Field-emission transmission electron microscopy (FE-TEM) images of ε-Fe$_2$O$_3$ NPs embedded in SiO$_2$ particles after annealing at 1180 °C for 4 h. (f) and (g) TEM images of the corresponding ε-Fe$_2$O$_3$ NPs after SiO$_2$ removal.

Fig. 1(b) and (c), the as-spray-dried microspheres exhibit hollow spherical structures induced by drying the ethanolic solvent mixture.[16] Post-annealing of the precursor particles in air induces the formation of iron oxide NPs in the hollow microspheres, as shown in the field-emission TEM images (Fig. 1(d) and (e)). Fe$_2$O$_3$ NPs are obtained after subsequent washing to remove the silica matrix (Fig. 1(f) and (g)).

Since the ε-phase is stable only in certain size regimes,[4] the annealing temperature and ratio between the Fe and silica precursor were varied to produce pure ε-Fe$_2$O$_3$. Fig. 2(a) and Fig. S1(a) (ESI†) provide representative X-ray diffraction (XRD) patterns and phase fractions of the obtained powders (Fe$_2$O$_3$@SiO$_2$). For the sample annealed in air at 930 °C for 4 h, the obtained pattern indicates only the γ-phase of Fe$_2$O$_3$ (ICDD No. 00-025-1402). As the temperature increases to 1050 °C, the intensity of the (122) peak of the ε-phase (ICDD No. 00-016-0653) significantly increases, and the (311) peak of the γ phase begins to decrease. A pure ε-Fe$_2$O$_3$ phase is observed at 1180 °C in Fig. S1(a) (ESI†). However, the powders treated at 1240 °C contain ε-Fe$_2$O$_3$ (59.4 wt%) and α-Fe$_2$O$_3$ (40.6 wt%) (ICDD No. 00-33-0664), which implies that the ε-phase partially transforms into α-Fe$_2$O$_3$ when the heating temperature increases. In addition, the obtained particle size significantly increases from 7.76 ± 1.7 nm to 56.77 ± 29 nm as the temperature increases (Fig. S2(a), ESI†). These results demonstrate that the Fe$_2$O$_3$ synthesized in this study displays a γ → ε → α phase transformation pathway
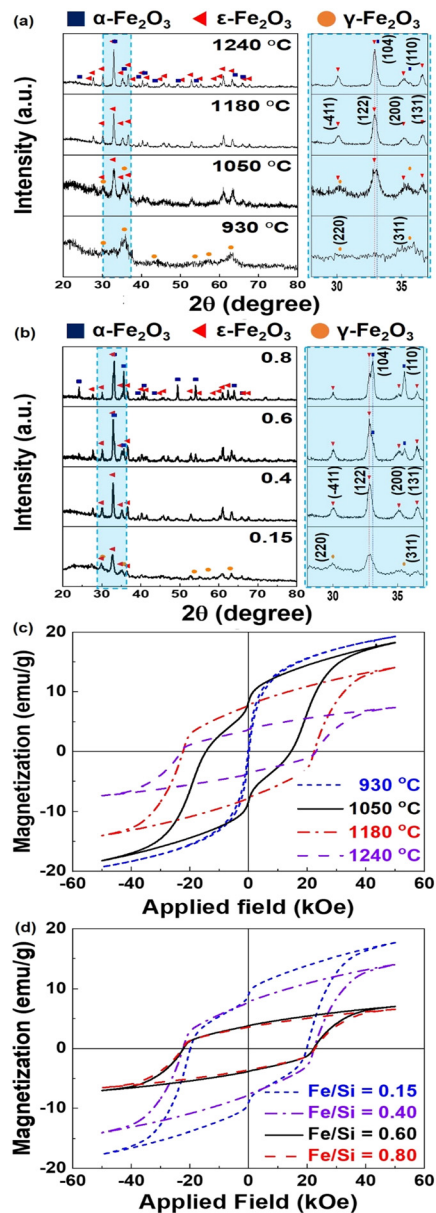

Fig. 2 XRD patterns of ε-Fe$_2$O$_3$ NPs@SiO$_2$ (a) annealed in air at various temperatures for 4 h using precursor particles with a precursor molar ratio (Fe/Si) of 0.4 : 1 and (b) prepared using various precursor molar ratios (Fe/Si) under the optimized annealing conditions (1180 °C, 4 h) and (c) and (d) magnetic hysteresis loops of ε-Fe$_2$O$_3$ NPs in (a) and (b) after SiO$_2$ removal.

as the heating temperature and particle size increase, which is analogous to the results of a previous study.[11]

We changed the Fe/Si molar ratio of the precursor under optimized heat-treatment conditions (1180 °C, 4 h). Fig. 2(b) and Fig. S1(b) (ESI†) demonstrate that powders with an Fe/Si molar ratio of ~0.15 comprise 14.0 wt% γ-Fe$_2$O$_3$ and 86.0 wt% ε-Fe$_2$O$_3$. As the ratio increases to 0.4, ε-Fe$_2$O$_3$ with a phase fraction of ~100 wt% is obtained. Above 0.6, sharp increases in the intensities of the (104) and (110) peaks of α-Fe$_2$O$_3$ and a decrease in the intensity of the (122) peak of ε-Fe$_2$O$_3$ are observed. Fig. S2(b) (ESI†) also demonstrates the dependence of the particle size on the Fe/Si molar ratio. As the Fe/Si molar

ratio increases, the particle size increases from 20.41 ± 3.8 nm to 57.54 ± 28 nm. The standard deviation of the size also increases for molar ratios greater than 0.60, owing to further formation of α-Fe_2O_3. The particle sizes obtained for high-purity ε-Fe_2O_3 (avg. 34.63 ± 11 nm) are within the size range of 8–40 nm that is desired to form a single ε-phase, as reported previously.[4] Based on the results, the optimized synthetic conditions (Fe/Si molar ratio = 0.4, annealing temperature = 1180 °C) were fixed to obtain a high-purity ε-phase, which was quantitatively analyzed using ^{57}Fe Mössbauer spectra. The four sextets for Fe sites corresponding to ε-Fe_2O_3 primarily exhibit one doublet for α-Fe_2O_3 (Fig. S3, ESI†).[6] The relative areas of ε-Fe_2O_3 and α-Fe_2O_3, which were obtained from the fitted Mössbauer parameters, were calculated to be 92.7% and 7.3%, respectively (Table S1, ESI†).

Thus, high-purity ε-Fe_2O_3 could be synthesized *via* an efficient aerosol-assisted method. To prepare the precursor solution, TEOS was mixed in an ethanolic mixture containing iron nitrate, which was hydrolyzed into silicic acid in a low-pH solution.[17] Rapid evaporation of the clear solution during spraying induced the instant formation of microparticles consisting of elemental Fe and Si. In the annealing step, the polymerization of hydrolyzed TEOS occurs first, creating an amorphous silica network in the microspheres.[18] Therefore, it was speculated that the Fe salt embedded in the densified silica underwent spatial confinement during heating. The excessive growth of iron oxide in the sphere could be restricted, causing the formation of the ε-phase. These results show that spray drying can be an efficient means of producing high-purity ε-Fe_2O_3 without the use of surfactants or sacrificial templates in a single step. Commonly, the duration of ε-Fe_2O_3 synthesis depends on the preparation of the composite of Fe salt and silica matrix. In particular, the time for hydrolysis and condensation of TEOS determines the time to form a silica matrix, which has taken 2–20 h in previous studies.[9,15] In contrast, spray drying involves the immediate evaporation of droplets combined with the continuous feeding of a precursor solution, which enables the reduction of the synthetic time with high yields. Furthermore, compared to the previously reported wet reaction conducted in a batch reactor,[9,14] this aerosol-assisted method enables continuous production of dried composite particles without washing or post-drying. Thus, this strategy provides an efficient and scalable manufacturing means of synthesizing ε-Fe_2O_3.

To elucidate the effects of the annealing temperature and precursor molar ratio on the magnetic properties, a magnetic property measurement system (MPMS) analysis of the obtained NPs after the removal of the silica matrix was performed. The M–H curves of the samples and corresponding coercivity (H_c), remanence (M_r), and maximum magnetization under the maximum applied field ($M_{5.0T}$) are presented in Fig. 2(c) and (d) and Table S2 (ESI†). The samples treated at 930 °C exhibit soft magnetic behavior of γ-Fe_2O_3 NPs with an average diameter of 7.76 ± 1.7 nm.[19] As the heating temperature increases to 1050 °C, a distinctive kink in the magnetic hysteresis loop (Fig. 2(c)) appears because of the coexistence of the ε- and γ-phases.

However, the oxide particles annealed at 1180 °C exhibit the typical magnetic behavior of ε-Fe_2O_3 with an exceedingly high H_c of more than 22 kOe. Above 1180 °C, $M_{5.0T}$ decreases with nearly stable H_c, which is related to the formation of the α phase.

The resulting powders prepared using various precursor molar ratios exhibit magnetic behavior depending on $\gamma \rightarrow \varepsilon \rightarrow \alpha$ phase transformation (Fig. 2(d)). The kink in the M–H curve observed at an Fe/Si ratio of 0.15 results from the soft magnetic γ phase with a fraction of ~ 14 wt% (Fig. S1(b), ESI†). As the Fe/Si ratio increases to 0.4, the kink disappears and hard magnetic behavior is observed with increasing H_c (over 22 kOe) and decreasing $M_{5.0T}$, resulting from complete phase transformation from the γ phase to the ε-phase. As the molar ratio increases from 0.40 to 0.80, hard magnetic behavior is observed with decreasing $M_{5.0T}$ owing to α-phase development. Based on the results, under the same heating conditions, control of the Fe/Si ratio enables modulation of the purity and magnetic properties of ε-Fe_2O_3, which originates from the size-driven phase transition of the ε-phase.[4,15] The resulting ε-Fe_2O_3 prepared under the optimized conditions shows similar magnetic properties (H_c = 22.4 kOe and $M_{5.0T}$ = 14.3 emu g^{-1}) to those reported for ε-Fe_2O_3 (Table S3, ESI†),[9] which indicates that this synthetic method can reproduce the excellent magnetic properties of ε-Fe_2O_3.

It is well known that ε-Fe_2O_3 with a large coercive field absorbs high-frequency EM waves because the zero-field ferromagnetic resonance is dependent on the magnetic anisotropy field.[7,8] In particular, nonmagnetic substitution of Fe enables the adjustment of the coercivities of ε-Fe_2O_3,[20,21] resulting in tunable ferromagnetic resonance from 30 GHz to 230 GHz.[9,10] Thus, to provide a proof-of-concept of the millimeter-wave absorber, we prepared Ga-substituted ε-Fe_2O_3 (ε-$Ga_xFe_{2-x}O_3$, $0.24 \leq x \leq 0.48$) *via* a spray drying method. All magnetic oxides formed a high-purity ε-phase, as shown in the XRD patterns in Fig. S4 (ESI†). The magnetic properties of the ε-$Ga_xFe_{2-x}O_3$ powders are presented in Fig. 3(a) and Table S4 (ESI†) for x = 0.24, 0.32, 0.42, and 0.48. H_c decreases from 22.3 kOe (x = 0) to 5.4 kOe (x = 0.48) as x increases. In addition, $M_{5.0T}$ increases from 14.2 emu g^{-1} (x = 0) to 26.3 emu g^{-1} (x = 0.42) and then decreases to 23.5 emu g^{-1} (x = 0.48). These results are in accordance with those of a previous study (Table S3, ESI†), showing that substituting ε-Fe_2O_3 with nonmagnetic ions adjusts the magnetic properties.[8,9] The absorbing composite films were prepared by mixing ε-Fe_2O_3 NPs and thermoplastic urethane (TPU) at a ε-$Ga_xFe_{2-x}O_3$:TPU weight ratio of 8:2 (Fig. S5; see ESI†). EM absorption spectra and permeability values in the range 60–110 GHz were measured for the films using a vector network analyzer. Strong absorption of the ε-$Ga_xFe_{2-x}O_3$ composite films is observed in Fig. 3(b). The resonant frequencies (f_r) of the magnetic composites shift from 105 GHz to 71 GHz with increasing Ga substitution (105 GHz (x = 0.24), 93 GHz (x = 0.32), 82 GHz (x = 0.42), and 71 GHz (x = 0.48)). These findings are in accordance with those of previous studies, demonstrating that nonmagnetic substitution changes the magnetocrystalline anisotropy, resulting in tunable ferromagnetic resonance characteristics.[7-10] The corresponding
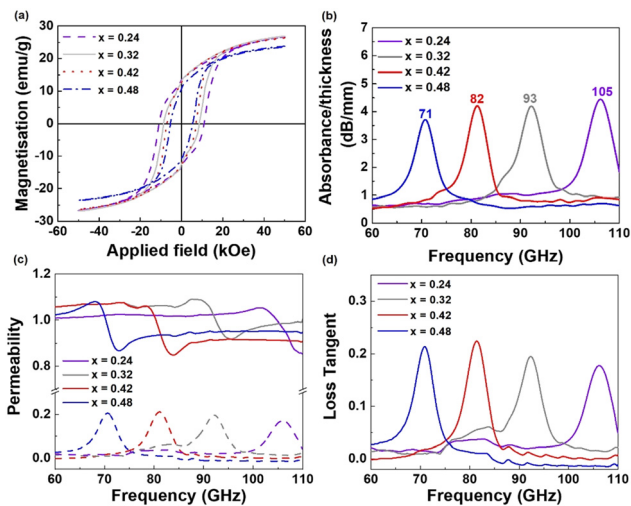
Fig. 3 (a) Magnetic hysteresis loops of ε-Ga$_x$Fe$_{2-x}$O$_3$ (0.24 ≤ x ≤ 0.48) powders. (b) Millimeter-wave absorption spectra normalized by film thickness. (c) Real (μ') and (d) imaginary (μ'') parts of magnetic permeability obtained from ε-Ga$_x$Fe$_{2-x}$O$_3$-based TPU composite films. The EM absorption properties were measured under zero magnetic field at room temperature. In the x = 0.24 sample, the absorption peak exceeds the measurement range.

permeability and permittivity values of the ε-Ga$_x$Fe$_{2-x}$O$_3$ composite film are presented in Fig. 3(c) and Fig. S6 (ESI†).

A sudden decrease in the real permeability (μ') and spike in the imaginary permeability (μ') are observed. μ'' exhibits the maximum value at each resonant frequency, which is attributed to natural resonance.[20] The magnetic loss tangent describes the power lost *versus* the power stored (tan $\delta_m = \mu''/\mu'$), which implies energy dissipation in each composite film.[22] The loss tangent increases from 0 to approximately 0.2 in the ε-Fe$_2$O$_3$ films (Fig. 3(d)), which means that high absorption of EM waves occurs at each f_r. Therefore, magnetic iron oxide synthesized by spray drying has great potential as a millimeter-wave absorber for use in automotive radar systems, military applications, and next-generation wireless communication.

In this study, a simple and scalable method of synthesizing high-purity (92.7%) ε-Fe$_2$O$_3$ NPs with a large coercive field (∼22 kOe) was successfully developed. This synthesis approach based on rapid spray drying of the precursor solution enables the spatial confinement of Fe salts in silica microspheres, which restricts excessive crystal growth during the annealing step. The particle size required to form the ε-phase can be easily tuned by controlling the precursor molar ratio and annealing temperature. Thus, high-purity ε-Fe$_2$O$_3$ particles can be obtained *via* a simple, fast, and scalable process without utilizing surfactants or porous templates. Additionally, the use of a simple and continuous process to produce precursor powders can considerably reduce the duration of the synthetic process. Furthermore, the ability to absorb millimeter waves

was demonstrated using the ε-Fe$_2$O$_3$ composite film. This synthetic strategy is expected to pave the way for industrial applications of ε-Fe$_2$O$_3$ such as permanent magnets, magnetic recording media, information storage, and millimeter-wave absorbers for use in high-speed wireless communication.

Conflicts of interest

There are no conflicts to declare.

Notes and references

1 A. H. Lu, E. L. Salabas and F. Schüth, *Angew. Chem., Int. Ed.*, 2007, **46**, 1222–1244.
2 R. M. Cornell and U. Schwertmann, *The Iron Oxides: Structure, Properties, Reactions, Occurences and Uses*, John Wiley & Sons, 2003.
3 A. Namai, M. Yoshikiyo, K. Yamada, S. Sakurai, T. Goto, T. Yoshida, T. Miyazaki, M. Nakajima, T. Suemoto, H. Tokoro and S. Ohkoshi, *Nat. Commun.*, 2012, **3**, 1–6.
4 S.-i Ohkoshi, A. Namai, K. Imoto, M. Yoshikiyo, W. Tarora, K. Nakagawa, M. Komine, Y. Miyamoto, T. Nasu, S. Oka and H. Tokoro, *Sci. Rep.*, 2015, **5**, 14414.
5 J. Jin, S.-i Ohkoshi and K. Hashimoto, *Adv. Mater.*, 2004, **16**, 48–51.
6 J. Tucek, R. Zboril, A. Namai and S.-i Ohkoshi, *Chem. Mater.*, 2010, **22**, 6483–6505.
7 C. Kittel, *Phys. Rev.*, 1947, **71**, 270–271.
8 A. Namai, M. Yoshikiyo, S. Umeda, T. Yoshida, T. Miyazaki, M. Nakajima, K. Yamaguchi, T. Suemoto and S. Okoshi, *J. Mater. Chem. C*, 2013, **1**, 5200–5206.
9 S. Ohkoshi, S. Kuroki, S. Sakurai, K. Marsumoto, K. Sato and S. Sasaki, *Angew. Chem., Int. Ed.*, 2007, **46**, 8392–8395.
10 Y. Gu, N. J. O. Silva, M. Yoshikiyo, A. Namai, R. Pinol, G. Maurin-Pasturel, Y. Cui, S. Ohkoshi, A. Millan and A. Martinez, *Chem. Commun.*, 2021, **57**, 2285–2288.
11 S. Sakurai, A. Namai, K. Hashimoto and S.-i Ohkoshi, *J. Am. Chem. Soc.*, 2009, **131**, 18299–18303.
12 S.-i Ohkoshi and H. Tokoro, *Bull. Chem. Soc. Jpn.*, 2013, **86**, 897–907.
13 S. Sakurai, K. Tomita, K. Hashimoto, H. Yashiro and S.-i Ohkoshi, *J. Phys. Chem. C*, 2008, **112**, 20212–20216.
14 J. López-Sánchez, A. Serrano, A. del Campo, M. Abuín, E. Salas-Colera, A. Muñoz-Noval, G. R. Castro, J. de la Figuera, J. F. Marco, P. Marín, N. Carmona and O. Rodríguez de la Fuente, *RSC Adv.*, 2019, **9**, 17571.
15 E. Gorbachev, M. Soshnikov, M. Wu, L. Alyabyeva, D. Myakishev, E. Kozlyakova, V. Lebedev, E. Anokhin, B. Gorshunov, O. Brylev, P. Kazin and L. Trusov, *J. Mater. Chem. C*, 2021, **9**, 6713.
16 D. P. Debecker, S. Le Bras, C. Boissière and A. Chaumonnot, *Chem. Soc. Rev.*, 2018, **47**, 4112–4155.
17 A. Douy, *J. Eur. Ceram. Soc.*, 2006, **26**, 1447–1454.
18 S. Bruni, F. Cariati, M. Casu, A. Lai, A. Musinu, G. Piccaluga and S. Solinas, *Nanostruct. Mater.*, 1999, **11**, 573–586.
19 C. de Montferrand, Y. Lalatonne, D. Bonnin, N. Lièvre, M. Lecouvey, P. Monod, V. Russier and L. Motte, *Small*, 2012, **8**, 1945–1956.
20 R. Kinugawa, K. Imoto, Y. Futakawa, S. Shimizu, R. Fujiwara, M. Yoshikiyo, A. Namai and S. Ohkoshi, *Adv. Eng. Mater.*, 2021, 2001473.
21 S. Ohkoshi, K. Imoto, A. Namai, S. Anan, M. Yoshikiyo and H. Tokoro, *J. Am. Chem. Soc.*, 2017, **139**(38), 13268–13271.
22 Y.-K. Hong and J. Lee, *Solid State Phys.*, 2013, **64**, 237–329.